Hindawi
Mathematical Problems in Engineering
Volume 2022, Article ID 7157334, 14 pages
https://doi.org/10.1155/2022/7157334

Research Article

Mathematical Model for Energy and Exergy-Based Simulation of Triangular Solar Energy Extractor for Air Heating Applications

C. Ramesh,[1] M. Vijayakumar,[2] L. Jeyanthi,[3] P. L. Rupesh,[4] A. Kanchana,[5] P. R. Jyothi Sankar,[6] V. S. Sajith,[7] Neha Munjal,[8] and Habtewolde Ababu Birhanu[9]

[1]*Department of Mechanical Engineering, KIT-KalaignarKarunanidhi Institute of Technology, Coimbatore 641402, Tamilnadu, India*
[2]*Department of Mechanical Engineering, PSN College of Engineering and Technology, Tirunelveli 627152, Tamilnadu, India*
[3]*Department of Mathematics, Panimalar Engineering College, Chennai 600123, Tamilnadu, India*
[4]*Department of Mechanical Engineering, Vel Tech Rangarajan Dr Sagunthala R&D Institute of Science and Technology, Chennai 600062, Tamilnadu, India*
[5]*Department of Mathematics, Rajalakshmi Institute of Technology, Chennai 600124, Tamilnadu, India*
[6]*Department of Mechanical Engineering, NSS College of Engineering, Palakkad 678008, Kerala, India*
[7]*Department of Mathematics, NSS College of Engineering, Palakkad 678008, Kerala, India*
[8]*Department of Physics, Lovely Professional University, Phagwara 144411, Punjab, India*
[9]*Faculty of Mechanical Engineering, Arba Minch Institute of Technology, Arba Minch University, P.O. Box 21, Arba Minch, Ethiopia*

Correspondence should be addressed to Habtewolde Ababu Birhanu; habtewold.ababu@amu.edu.et

Received 24 March 2022; Revised 9 April 2022; Accepted 13 April 2022; Published 7 June 2022

Academic Editor: Ravi Samikannu

In the present work, the thermal and exergy efficiency of the equilateral triangular duct solar air heater is analytically investigated and its performance is improved by attaching an inclined wire rib over the absorber surface. Using triangular ducts improves the operating flow conditions up to the Reynolds number of 35000. The thermal model of solar air heater is solved by using an iterative procedure by code developed in MATLAB. The analysis considers the roughness parameters that roughness pitch (P)-to-height (e) ratio (P/e) of 4 to 16, roughness height (e)-to-hydraulic diameter (D_h) ratio (e/D_h) of 0.021 to 0.043, and rib inclination angle (α) of 30 to 75°. While increasing the Reynolds number from 2000 to 35000, the inclined rib roughened triangular duct solar air heater thermal performance is increased and attains the maximum value of 83.61% and the effective thermal efficiency of 80.26%. The maximum exergy efficiency of 2.62% is obtained at the Reynolds number value of 1864. It improves the thermal performance by 14.2% as compared with the rectangular rib roughened triangular duct solar air heater. The optimum value of roughness parameters is P/e of 12, e/D of 0.042, and α of 75°. The air heater is useable to attain the temperature rise parameter ranges from 0.001 to 0.03 K·m^2/W.

1. Introduction

Industries in developing countries are unsustainable because of the rapid escalation in the emission of greenhouse gases [1]. Therefore they are formulating their new energy policy to encourage eco-friendly energy usage for sustainable development. The researchers and economists identified the potential of solar thermal technologies specifically for industries for sustainable operations and production of low carbon emissions [2]. Among the industrial solar heat production devices, the flat plate solar air heaters are applicable for low temperature heating processes with an operating temperature range of 60 to 85°C [3].

The thermal performance improvement in rectangular duct solar air heaters is achieved by incorporating the techniques like artificial roughness, jet impingement, fins, and baffles [4]. The thermal performance enhancement techniques raise fluid friction and improve the pumping

power consumption. The researchers also utilized novel roughness shapes such as winglike tabulators [5], trapezoidal louvered winglets with wavy grooves [6], and double pass [7] arrangements to maximize the thermos hydraulic performance of rectangular duct solar air heater. These techniques effectively improve the heat transfer rate with a penalty of higher consumption in pumping power. Then it is identified that usage of triangular flow passages lowers the pressure drop and minimizes the consumption of pumping power [8]. The triangular ducts can integrate with artificial roughness and can produce a better performance as compared with conventional ducts. The influence of apex angle and dimple roughness on heat transfer and frictional characteristics of triangular air heater was experimentally investigated by Goel et al. and revealed that an apex angle of 60° makes the system more efficient [9]. Kumar et al. improved the thermohydraulic features of triangular duct channels by incorporating semicircular ribs and concluded that lower pitch distance and higher roughness height values improved the system performance by 2.2 times as compared with conventional system [10]. The provision of the rounded corner and straight ribs on triangular channels are investigated by Kumar et al. who observed the performance augmentation by 2.48 times at the Reynold number of 18000 and the relative roughness pitch value of 12 [11]. The researchers also investigated the aspect ratio of straight ribs suitable for triangular channels and concluded that providing the aspect ratio rib roughness values of 4.0 improves the hydraulic performance parameter by 1.89 times as compared with earlier studies [12].

Bharadwaj et al. [13] experimentally analyzed the heated triangular duct by using inclined rib roughness and suggested formulating a correlation between energy transfer and frictional factors as a function of inclined rib roughness parameters. Singh [14] uses recycling and discrete V ribs on TDSAH and concluded that the maximum thermohydraulic performance of the system was 71% at the hydraulic diameter of 0.06 m with a temperature rise parameter of 0.004 kW/m^2. Kumar et al. [15] also investigated the roughened triangular airflow channels by using CFD analysis for the roughness profiles of elliptical, rectangular, and circular ribs. While comparing the results, it is concluded that the rectangular ribs have superior performance that yields around 1.89 times improvement in thermohydraulic performance [16]. Kumar et al. [17] further carried out a thermal performance investigation in this field by varying the radius of curvature (R_c) of the duct and identified that R_c of 0.33 h provides the enhancement by 21 to 25%. Jain et al. [18] incorporated broken inclined ribs on equilateral triangular ducts and carried out the numerical analysis and revealed that relative gap positions with a value of 0.25 provide the thermohydraulic performance parameter of 2 for the Reynolds number ranging from 4000 to 8000.

Nidhul et al. [19] carried out an exegetic performance of TDSAH with the integration of V-shaped rib roughness for the Reynolds number ranges from 5000 to 20000 and concluded that an effective rib angle of 45° yields the maximum exergetic performance of the collector of 2.3%. Misra et al. [20] modified this V shape design with multiple gaps and carried out the investigation numerically for roughness pitch and angle of attack varies from 8 to 14 and 45 to 60°, respectively. Among these conditions, roughness pitch of 10 and angle of attack of 45 formulate better turbulence with a minimum formulation of eddy viscosity. Nidul et al. [21] carried out exergetic performance using an analytical model for straight rectangular ribs and concluded that the enhancement in thermal and exergy efficiency by 36 and 17% for the rib aspect ratio of 4. Kumar et al. [22] compared the exergetic performance of semicircular and square straight ribs and resulted that semicircular ribs enhance the performance by 26%.

The analytical and experimental investigations available in triangular duct solar air heaters have been summarized in Table 1. However, it was noted that heat transfer and friction factor analysis were considered for the analysis of artificially roughened TDSAH and less work is conveyed on the first law, effective thermal and exergy based analysis. From the table, it was noticed that exergy based performance analysis was considered for the roughness shaped of straight rectangular, semicircular, and V ribs. These designs result in lower enhancements of thermal performance on SAH.

The literature studies also recognized that the influence of artificial roughness with inclined circular ribs is not investigated based on its thermohydraulic and exergetic performance. There is very lesser analysis carried out for triangular air heaters to evaluate its realistic performance on exergy basis. The objective of this work is to improve the performance of solar air heater and investigate the effective thermal and exergetic performance by using inclined circular ribs on triangular duct solar air heaters. The configuration is stated as an inclined rib roughened triangular duct solar air heater (IRTDSAH). During this analysis, the influence of roughness pitch (P) to height (e) ratio (P/e), roughness height (e) to hydraulic diameter (D_h) ratio (e/D_h), and rib inclination angle (α) on effective thermal and exergy efficiency is investigated to identify its optimum values.

2. Theoretical Analysis

The inclined rib roughened triangular duct solar air heater is illustrated in Figure 1(a). Three identical size plates that are to be considered backplates and absorber plates create the airflow path for the air heater. The triangular channel is covered by insulation at the bottom and sides and a transparent glass cover at the top to minimize heat losses. The inclined wire ribs are attached at the bottom of the absorber plate to act as a tabulator for improving the convection current. The details of the inclined wire ribs and the operating parameters are described in Figure 1(b). The inclined rib attached over the absorber plate breaks the sublayer formulation, and the pitch between the plates and its inclination angle supports flow separation in upstream and flow reattachment in downstream conditions.

3. Energy-Based Performance of IRTDSAH

3.1. Thermal Efficiency. The real usability of IRTDSAH is calculated by considering the quantity of thermal energy

Table 1: Particulars of reported research on artificially roughened triangular duct solar air heater.

Roughness design	Heat transfer and friction factor analysis	First law based energy and effective thermal performance	Second law based exergy analysis
Dimple shape	Goel et al. [9]	×	×
Straight semi-circular rib	Kumar et al. [10]	Kumar et al. [22]	Kumar et al. [22]
Straight circular rib	Kumar et al. [11]	×	×
Straight rectangular rib	Kumar et al. [12]	×	Nidhul et al. [21]
Inclined circular rib	Bharadwaj et al. [13]	×	×
Inclined broken square rib	Jain et al. [18]	×	×
V rib	Nidhul et al. [19]	×	Nidhul et al. [19]
V rib with multiple gap	Misra et al. [20]	×	×

flowing inwards to the system through the glass cover and the amount of heat that bring back to the ambient.

It is evaluated by considering the assumption that the roughened absorber plate is working at a mean temperature of T_{wf} and a surrounding temperature of T_{as} [23].

$$Q_{u1} = F_R A_C \left[I(\alpha\tau) - U_L \left(T_{wf} - T_{as} \right) \right]. \tag{1}$$

In the above equation, T_f is given by the following:

$$T_{wf} = \frac{T_{wfi} + T_{wfo}}{2}. \tag{2}$$

The rise in enthalpy of outlet air describes the energy gained by the working fluid evaluated using the relation as follows:

$$Qu_1 = m_{wf} C_{pf} \left(T_{wfo} - T_{wfi} \right). \tag{3}$$

Heat removal factor F_R from the roughened absorber plate is stated as follows [21]:

$$F_R = \frac{m_{wf} C_{pf} \left(T_{wfo} - T_{wfi} \right)}{A_C \left[I(\tau\alpha) - U_L \left(T_{wf} - T_{as} \right) \right]}. \tag{4}$$

The thermal performance of IRTDSAH can be calculated by using the equation stated by Hottel-Whiler-Bliss by using the parameters that cumulative heat loss coefficient U_L and heat removal factor F_R. It is stated as follows [24]:

$$\eta_{th} = \frac{Q_{u_1}}{I A_C} = F_R \left[I(\tau\alpha) - U_L \left(\frac{T_{wf} - T_{sa}}{I} \right) \right]. \tag{5}$$

Heat removal factor F_R in terms of collector efficiency factor is stated as follows:

$$F_R = \frac{m C_p}{U_L A_c} \left[1 - \exp\left(\frac{U_L A_p F'}{m C_p} \right) \right]. \tag{6}$$

3.2. Effective Thermal Efficiency. The effective thermal efficiency indicates the performance of IRTDSAH by considering the pumping power losses consumed by the system. It is evaluated by using the equation (7), which consists of efficiency of blower (η_B), efficiency of motor (η_m), efficiency of transmission (η_T), and power plant (η_P) [25].

$$\eta_{EE} = \frac{Q_{u1}}{I A_C} - \frac{P_m}{I A_C \left(\eta_B \eta_m \eta_T \eta_P \right)}. \tag{7}$$

3.3. Exergy Analysis. Exergy refers to the conversion of available energy into useful energy or work, and so exemplifies the compactness of the solar air heater. Exergy efficiency can also be stated as useful work that a system may produce with respect to the ambient, and it is defined as follows [26]:

$$\eta_{ex} = \frac{E_u}{E_{sun}}, \tag{8}$$

where E_u represents useful exergy output from RTDSAH and E_{sun} exergy input to the system from the Sun. It can be evaluated using the relation as follows [26]:

$$\dot{E}_{sun} = A_c I \left(1 - \frac{4}{3} \left(\frac{T_{fo}}{T_{sun}} \right) + \frac{1}{3} \left(\frac{T_{fo}}{T_{sun}} \right)^4 \right). \tag{9}$$

Equation (10) evaluates the irreversibility produced by loss of pressure and energy transfer to the air in the system. It is evaluated as follows:

$$\dot{E}_u = Q_{u1} - \dot{m}\, C_p T_o \cdot \ln\left(\frac{T_{fo}}{T_{fi}} \right) - \dot{m} T_o \, \frac{\Delta P}{\rho_f T_{fi}}, \tag{10}$$

where ΔP is the pressure drop that happens across the solar air heater path.

The entropy values describe the energy destruction from the solar air heater that is not able to convert as useful heat with respect to corresponding operating conditions and ambient temperature. It is evaluated using the following equation:

$$\text{Entropy} = \frac{E_{sun} - E_u}{T_a}. \tag{11}$$

3.4. Analytical Procedure. The energy and exergy analysis of IRTDSAH was evaluated by considering assumptions as follows [27].

(1) The energy and exergy investigations are carried out at the 1D-steady state model.

(2) There is a negligible temperature drop that happens across the components of IRTDSAH.

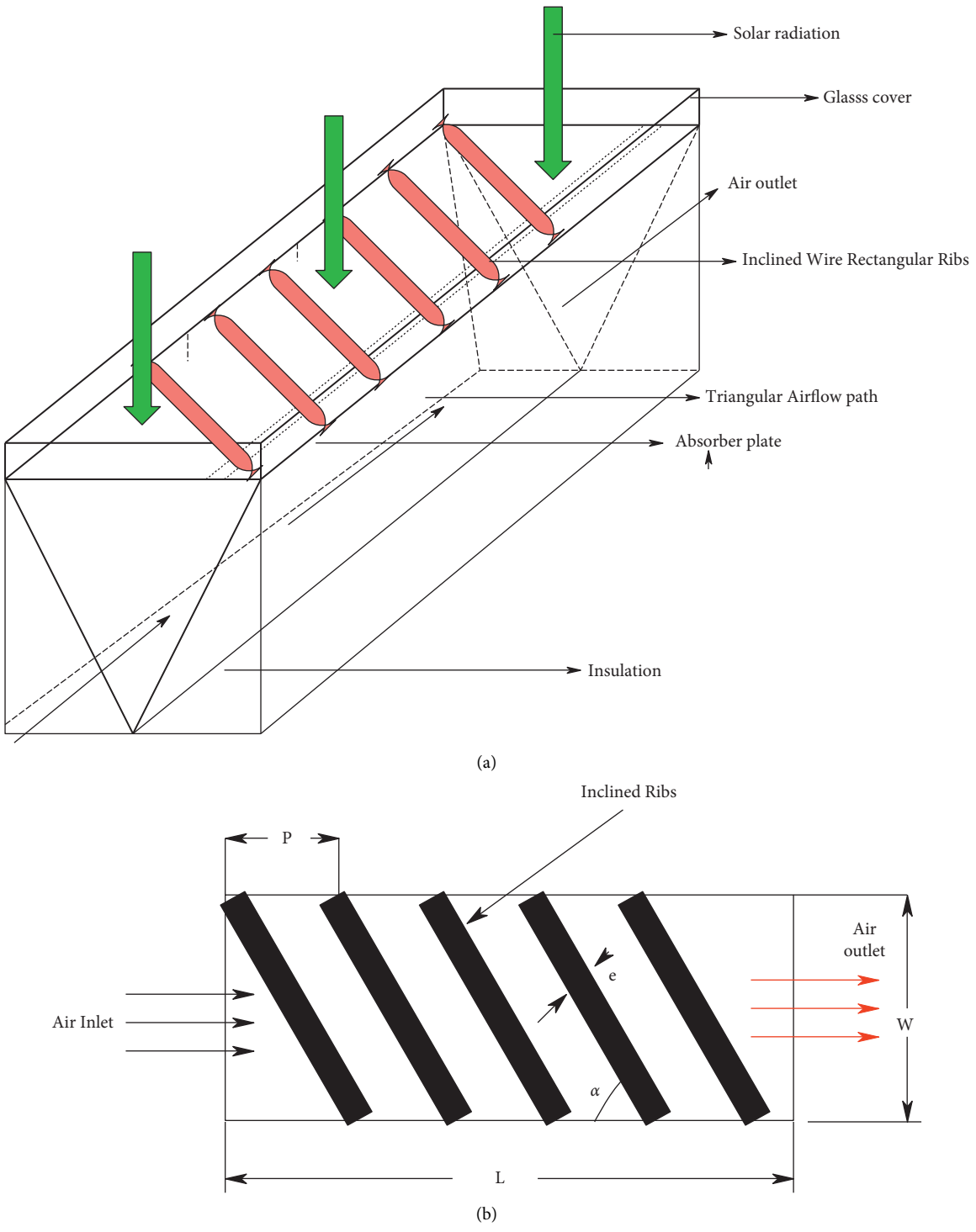

Figure 1: (a) Inclined rib roughened triangular duct solar air heater. (b) Roughness details.

(3) The joints of the air heater are leak-proof.

(4) The variation in convective heat transfer is coefficient across the length of the collector or negligible.

(5) Energy transfer that happens in the axial direction of the collector is only considered for evaluate the outlet temperature of air.

The thermal modeling procedure to evaluate the energy and exergetic performance of IRTDSAH is described below.

Step 1: The design parameters of inclined wire roughness and surrounding and operating conditions of SAH are taken from Table 2.

Table 2: Typical value of design and operating conditions.

Design and operating parameters	Value
Length (L) and width (W) of the duct	1.5 m
Thickness (δ_i) of insulation	0.06 m
Glass transparent cover thickness (t_g)	0.004 m
Thermal conductivity value of insulation (k_i)	0.04 W/mK
Thermal conductivity value of glass cover (k_g)	0.75 W/mK
Radiation of intensity (I)	1000 W/m^2
Atmospheric temperature (T_a)	300 K
Temperature rise parameter ($\Delta T/I$)	0.002–0.03 K·m^2/W
Reynolds number (Re)	2000–35000
Relative roughness height (e/D_h)	0.021–0.043
Relative roughness pitch (P/e)	4–16
Inclination angle of arc (α)	30–75°

Step 2: It is assumed that the air sucked from the surroundings to the inlet of the SAH is in thermal equilibrium with ambient air temperature. Therefore, the rise in temperature at the outlet (T_{fo}) of the air is evaluated by the following:

$$T_{fo} = T_{fi} + \Delta T. \tag{12}$$

Here ΔT represents the rise in temperature of air from the absorber surface. It is used to evaluate the rise in temperature ($\Delta T/I$) [18, 19, 28].

$$\Delta T = \frac{\Delta T}{I} \times I. \tag{13}$$

Step 3: Then equations (10)–(12) are used to evaluate the thermophysical properties of air [25].

$$\mu = 0.181 \times 10^{-4}\left(\frac{T_{wf}}{293}\right)^{0.735}, \tag{14}$$

$$C_p = 0.1006 \times 10^{4}\left(\frac{T_{wf}}{293}\right)^{0.0155}, \tag{15}$$

$$k = 0.275 \times 10^{-3}\left(\frac{T_{wf}}{293}\right)^{0.086}. \tag{16}$$

Step 4: The mean temperature of the absorber surface is estimated by using the equation as follows [26]:

$$T_{ap} = \frac{T_{fo} + T_{fi}}{2} + 10. \tag{17}$$

Step 5: The wasted heat losses through the top cover, back insulations, and side cover of the IRTDSAH due to convection are named as overall heat loss that is evaluated by using the relation [18, 19].

$$U_l = U_t + U_b + U_e. \tag{18}$$

In the above relation (18), U_b, Ut and U_e represent bottom, top, and side losses that happen in the SAH. The top loss of the SAH is influenced by the parameters of wind velocity, glass, and absorber plate temperature. Akhtar and Mullick correlation describes the top loss as follows [22]:

$$U_t = \left[\frac{\sigma\left(T_{ap}{}^2 + T_{gc}{}^2\right)\left(T_{ap} + T_{gc}\right)}{\left(1/\varepsilon_{ap}\right) + \left(1/\varepsilon_{gc}\right) - 1} + \left(\frac{kNu_l}{L_1}\right)\right] + \left[\sigma\varepsilon_g\left(T_{ap}{}^2 + T_{gc}{}^2\right)\left(T_{gc} + T_a\right) + h_w\right]^{-1} + \frac{t_{gc}}{k_{gc}}. \tag{19}$$

The terms in equation (16) are evaluated using the relations as follows:

$$T_{gc} = \left[\frac{F_l T_{ap} + cT_{as}}{1 + F_l}\right]$$

$$Nu_l = 1 + 1.44\left[1 - \frac{1708}{Ra\cos\beta}\right] + \left[1 - \frac{1708(\sin 1.8\,\beta)^{1.6}}{Ra\cos\beta}\right] + \left[\left(\frac{Ra\cos\beta}{5830}\right)^{0.33} - 1\right]$$

$$F_l = \frac{\left[12 \times 10^{-8}\left(T_{as} + 0.2T_{ap}\right)^3 + h_w\right]^{-1} + 0.3L_g}{\left[6 \times 10^{-8}\left(\varepsilon_{ap} + 0.028\right) \times \left(T_{ap} + 0.5T_{as}\right)^3 + 0.6L_1{}^{-0.2}\left\{\left(T_{ap} - T_{as}\right)\cos\beta\right\}^{0.25}\right]^{-1}} \tag{20}$$

$$c = \left[\frac{\left(T_{sky}/T_{as}\right) + \left(h_w/3.5\right)}{1 + \left(h_w/3.5\right)}\right]$$

$$T_s = 0.0522 \times \left(T_a\right)^{1.5}.$$

The edge and bottom losses from the system are evaluated using the relation as follows [21]:

$$U_b = \frac{k_i}{\delta_i},$$
$$U_e = \frac{t_e k i}{\delta_i} \times \left[\frac{3a}{(1/2) \times aH}\right]. \tag{21}$$

Step 6: The useful energy gain from the IRTDSAH is given by the following:

$$Q_{u1} = A_c\left[I(\tau\alpha) - U_L\left(T_{ap} - T_{as}\right)\right]. \tag{22}$$

Step 7: The mass flow rate that happens in the IRTDSAH is evaluated by the following equations [21]:

$$\dot{m} = \frac{Q_{u_1}}{C_p \Delta T}, \tag{23}$$

$$\mathrm{Re} = \frac{\dot{m} D_h}{\mu A_{cs}}. \tag{24}$$

Step 8: Then the convective heat transfer coefficient of IRTDSAH is calculated based on the Nusselt number correlation that incorporates the relation between the nondimensional inclined wire roughness design parameters is as follows [13]:

$$Nu = 0.0031\left[\mathrm{Re}^{1.0972}\left(\frac{P}{e}\right)^{1.0832}\left(\frac{\alpha}{60}\right)^{0.0792}\left(\frac{e}{D_h}\right)^{0.3585} \times \exp\left\{-0.1908\left(\ln\left(\frac{\alpha}{60}\right)\right)^2\right\} \times \right] \exp\left\{-0.246\left(\ln\left(\frac{P}{e}\right)\right)^2\right\},$$
$$h_c = \frac{Nuk_a}{D_h}. \tag{25}$$

Step 9: The plate efficiency factor F′ is calculated by using the value of convective heat transfer coefficient value h_c and the heat loss coefficient value of UL by using the relation shown below [21]:

$$F^{\prime} = \frac{h_c}{h_c + U_L}. \tag{26}$$

Step 10: The outlet temperature based heat gain value (Qu_2) is calculated using the equation as mentioned below [21, 22]:

$$Q_{u2} = F_R A_c\left[I(\tau\alpha) - U_L\left(T_{fo} - T_{fi}\right)\right]. \tag{27}$$

Step 11: Then, the deviation between Q_{u2} and Q_{u1} is evaluated. If the difference between the heat gain values is more than 0.01%, then the mean plate temperature of the IRTDSAH is recalculated and resubstituted by equations (22) and (28). The procedure is repeated from the sequence of steps 4 to Step 10 up to the attainment of convergence [26].

$$T_{ap} = T_{as} + \frac{\left[I(\alpha\tau) - \left[Q_{u2}/A_C\right]\right]}{U_L}. \tag{28}$$

Once the convergence is achieved, then the energy efficiency of the SAH is evaluated using equation (5).

Step 12: The frictional flow resistance occurred by the inclined rob roughness is evaluated by using the correlations, and the pump power requirement for propelling the air is given by the following [13]:

$$fr = 11.845\left[\mathrm{Re}^{-0.693}\left(\frac{P}{e}\right)^{1.1389}\left(\frac{\alpha}{60}\right)^{0.0418}\left(\frac{e}{D_h}\right)^{0.3365} \times \exp\left\{-0.1686\left(\ln\left(\frac{\alpha}{60}\right)\right)^2\right\} \times \right] \exp\left\{-0.2644\left(\ln\left(\frac{P}{e}\right)\right)^2\right\}. \tag{29}$$

Step 13: The evaluated friction factor from equation (29) is substituted in equation (30) to estimate the pressure drop (ΔP) and loss of pumping power (P_{m}) that occurs in IRTDSAH [27].

$$\Delta P = \frac{4 fr L v^2 \rho}{2 D_h}, \tag{30}$$

$$P_m = \frac{m \Delta P}{\rho}. \tag{31}$$

The effective thermal efficiency based performance of the IRTDSAH is evaluated by using the relation stated in equation (7).

4. Results and Discussion

The inclined rib roughened triangular duct solar air heater is analytically investigated and the influence of roughness pitch (P) to height (e) ratio (P/e), roughness height (e) to hydraulic diameter (D_{h}) ratio (e/D_{h}), and rib inclination angle (α) on thermal, effective and exergy efficiency of the IRTDSAH are presented in following sections.

4.1. Effect of Rib Roughness Angle (α) on Thermal Performance of IRTDSAH. The wire ribs are mounted on the IRTDSAH absorber plate with the inclination of angle α varies from 30° to 75°, and its effects on the thermal effective thermal and exergy efficiency are shown in Figures 2–7.

Figure 2 reveals the impact of rib roughness angle (α) ranges from 30 to 75° on the thermal efficiency of IRTDSAH, while flowing of air at the Reynolds number from 2000 to 35000, and maintaining other roughness parameters are constant, i.e., $e/D_{\mathrm{h}} = 0.043$ and $P/e = 12$. While increasing the Reynolds number from 2000 to 35000, the thermal efficiency of IRTDSAH improved by a maximum of 52.8% to 83.8% for the rib inclination angle (α) value of 75°. While decreasing the value of α decreases the thermal performance of IRTDSAH due to the production of thermally dead zones.

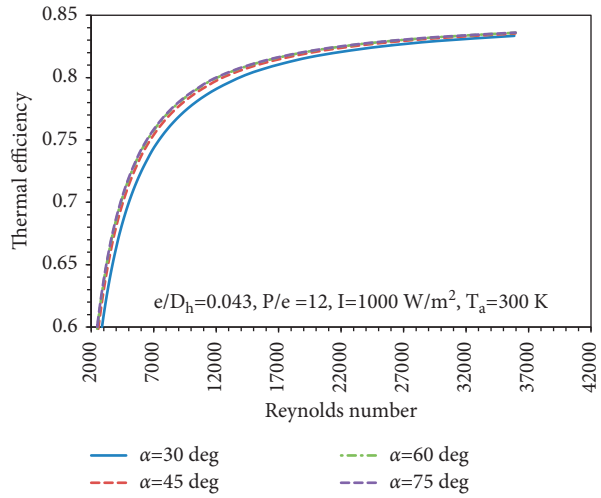

Figure 2: Impact of rib roughness angle (α) and Reynolds number on the thermal efficiency of IRTDSAH.

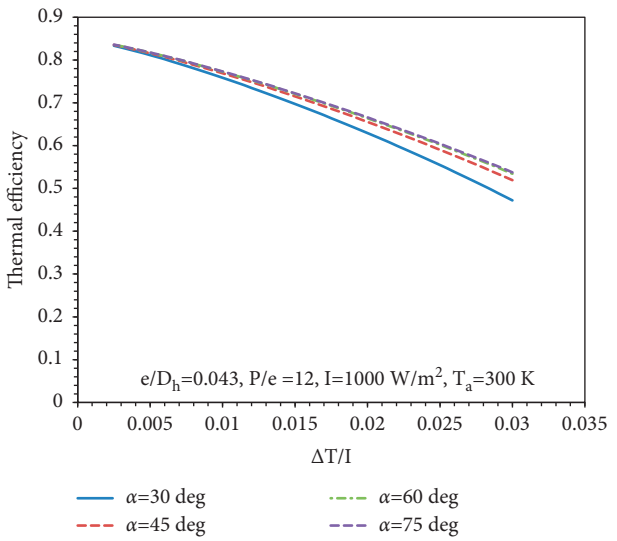

Figure 3: Impact of rib roughness angle (α) and rise in temperature parameter on thermal efficiency of IRTDSAH.

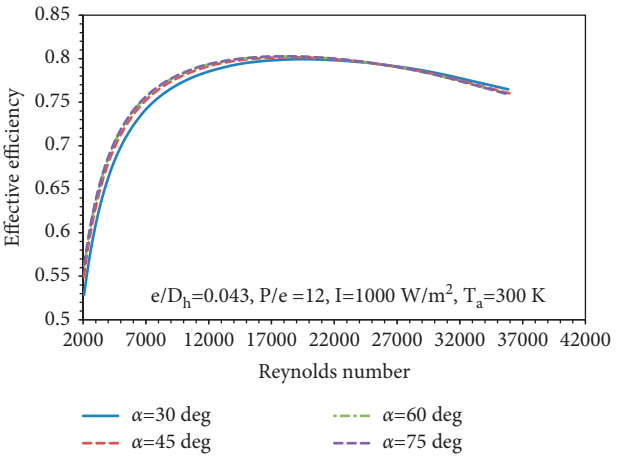

Figure 4: Impact of rib roughness angle (α) and Reynolds number on the effective thermal efficiency of IRTDSAH.

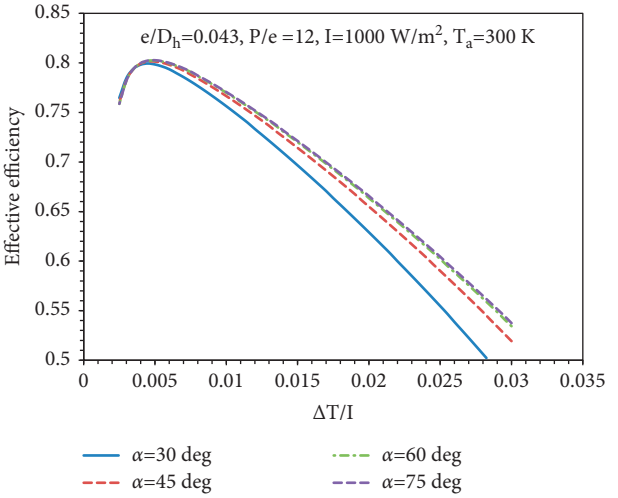

Figure 5: Impact of rib roughness angle (α) and rise in temperature parameter on the effective thermal efficiency of IRTDSAH.

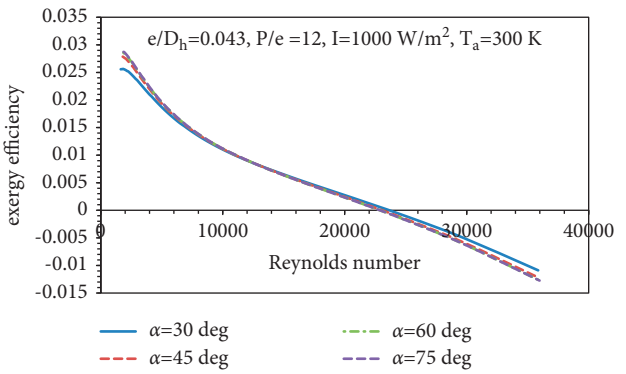

Figure 6: Impact of rib roughness angle (α) and reynolds number on exergy efficiency of IRTDSAH.

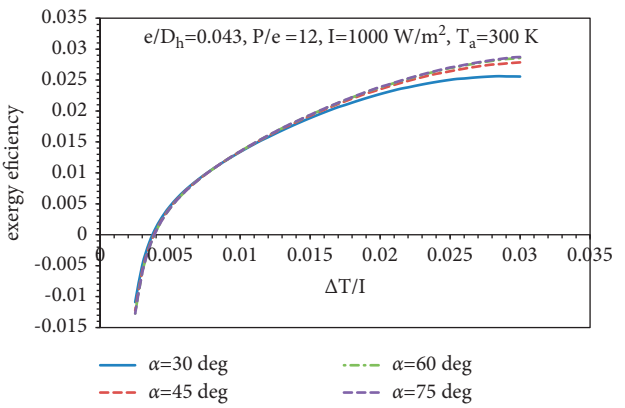

Figure 7: Impact of rib roughness angle (α) and rise in temperature parameter on exergy efficiency of IRTDSAH.

Figure 3 reveals the impact of rib roughness angle (α) ranging from 30 to 75° on the thermal efficiency of IRTDSAH while producing hot air with a rise in temperature parameter value ranging from 0.001 to 0.03 K·m^2/W and maintaining other roughness parameters are constant, i.e., *e*/

$D_h = 0.043$ and $P/e = 12$. The thermal efficiency values were found to increase with the increase in α. The maximum thermal efficiency value found in the analysis is 83.61% at $\alpha = 75^\circ$. Comparatively at a higher angle of attack, the thermal efficiency is higher because of effective flow reattachment in the boundary layer.

Figure 4 reveals the impact of rib roughness angle (α) ranges from 30 to 75° on the effective thermal efficiency of IRTDSAH, while flowing of air at the Reynolds number from 2000 to 35000, and maintaining other roughness parameters are constant, i.e., $e/D_h = 0.043$ and $P/e = 12$. The effective efficiency values found increases up to the critical Reynolds Number as shown in Table 3. The maximum effective efficiency value found in the analysis is 80.26% in $\alpha = 75^\circ$ at 17534 Reynolds number. For the same Reynolds number with $\alpha = 30^\circ$ the effective efficiency is 79.94%, while the trend gets reversed at higher Reynolds numbers (>25000) that $\alpha = 30^\circ$ yields better performance due to offering lesser flow resistance and consumption of lower pumping power. At a higher Reynolds Number, the pressure drop increases due to the turbulent flow nature of the air. Due to this reason, there is a dip in effective efficiency after the 17528 Reynolds Number. Comparatively, at a higher angle of attack, the effective efficiency is higher, which is evident.

Figure 5 reveals the impact of rib roughness angle (α) ranging from 30 to 75° on the effective thermal efficiency of IRTDSAH while producing hot air with a rise in temperature parameter value ranging from 0.001 to 0.03 K·m^2/W and maintaining other roughness parameters are constant, i.e., e/$D_h = 0.043$ and $P/e = 12$. The effective efficiency values found increase up to the critical value of rising in temperature parameter as shown in Table 4. The maximum effective efficiency value found in the analysis is 80.26% at $\alpha = 75^\circ$. Comparatively, at a higher angle of attack, the effective efficiency is higher.

Figure 6 reveals the impact of rib roughness angle (α) ranges from 30 to 75° on exergy efficiency of IRTDSAH, while flowing of air at the Reynolds number from 2000 to 35000, and maintaining other roughness parameters are constant, i.e., $e/D_h = 0.043$ and $P/e = 12$.

The exergy efficiency values were found to increase up to the critical value of the Reynolds number, as shown in Table 5. The maximum exergy efficiency value found in the analysis is 2.87% at $\alpha = 75^\circ$ at Re of 1864, and a further rise in Re > 1864 reduces the exergy efficiency. Comparatively, at operating the air heater lower angle of attack declines the second law efficiency of the system due to higher exergy losses and destructions at a lower Reynolds number. At the system operated at a Reynolds number >20000, it produces a negative value of exergy efficiency for all the values of α due to the rise in internal exergy destruction parameter such as fluid friction occurring between absorber plate and working fluid.

Figure 7 reveals the impact of rib roughness angle (α) ranges from 30 to 75° on exergy efficiency of IRTDSAH while producing hot air with a rise in temperature parameter value ranging from 0.001 to 0.03 K·m^2/W, and maintaining other roughness parameters are constant, i.e., $e/D_h = 0.043$ and $P/e = 12$. The exergy efficiency values were found to increase with the increase in $\Delta T/I$ and α till $\Delta T/I = 0.03$ K·m^2/W. The maximum exergy efficiency value found in the analysis is 2.87% at $\alpha = 75^\circ$. Comparatively, at a higher angle of attack, the exergy efficiency is higher. It is observed that at higher $\Delta T/I$, the exergy efficiency value increases.

Table 3: Critical Reynolds number based on different values of α.

S. no	α (°)	Maximum effective efficiency (%)	Reynolds number
1	30	79.94	19469
2	45	80.13	19551
3	60	80.24	17528
4	75	80.26	17534

Table 4: Influence of α on the rise in temperature parameter.

S. n	α (°)	$\Delta T/I$ for maximum effective efficiency	Maximum effective efficiency (%)
1	30	0.0045	79.94
2	45	0.005	80.13
3	60	0.005	80.24
4	75	0.005	80.26

Table 5: Critical reynolds number based on different values of α.

S. n	α (°)	Maximum exergy efficiency (%)	Reynolds number
1	30	2.56	1821
2	45	2.78	1801
3	60	2.85	1853
4	75	2.87	1864

4.2. Effect of Roughness Height (e)-to-Hydraulic Diameter (D_h) Ratio (e/D_h) on Thermal Performance of IRTDSAH. The wire ribs are mounted on the IRTDSAH absorber plate with roughness height to diameter ratio (e/D_h) varying from 0.021 to 0.042, and its effects on the thermal effective thermal and exergy efficiency are shown in Figures 8–14.

Figure 8 reveals the rib roughness height (e) to hydraulic diameter (D_h) ratio ranging from 0.021 to 0.043 on the thermal efficiency of IRTDSAH, while flowing of air at the Reynolds number from 2000 to 35000, and maintaining other roughness parameters are constant, i.e., $\alpha = 0.75^\circ$ and $P/e = 12$.

The maximum thermal efficiency value found in the analysis is 83.8% at $e/D_h = 0.043$. While increasing the Reynolds number from 2000 to 35000, the thermal efficiency of IRTDSAH improved by a maximum of 53.1% to 83.8% for the rib roughness height (e) to hydraulic diameter (D_h) ratio (e/D_h) value of 0.043. While decreasing the value of e/D_h decreases the thermal performance of IRTDSAH due to the poor formulation, secondary flow reattachment points at the downward part of IRTDSAH.

Figure 9 reveals the impact of rib roughness height (e) to hydraulic diameter (D_h) ratio from 0.021 to 0.043 on the thermal efficiency of IRTDSAH while producing hot air with a rise in temperature parameter value ranging from 0.001 to 0.03 K·m^2/W, and maintaining other roughness parameters are constant, i.e., $\alpha = 75^\circ$ and $P/e = 12$. The thermal efficiency

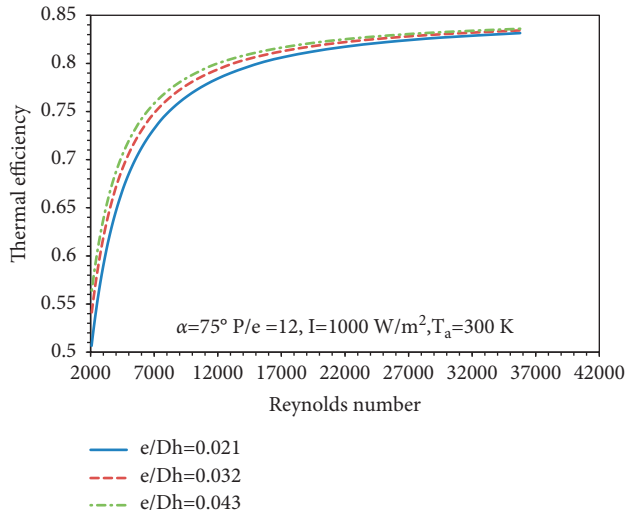

Figure 8: Impact of rib roughness height (e) to hydraulic diameter (D_h) ratio (e/D_h) and Reynolds number on the thermal efficiency of IRTDSAH.

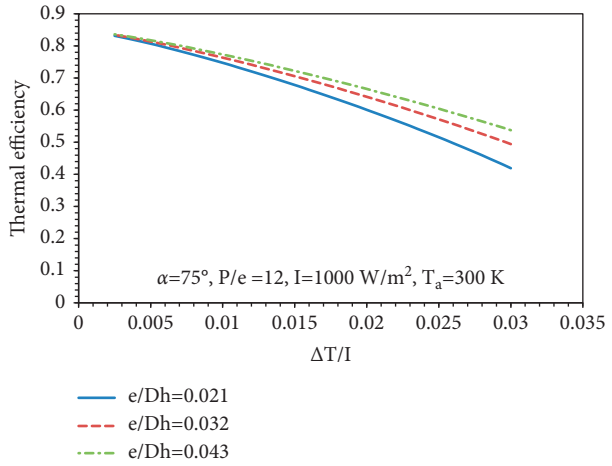

Figure 9: Impact of rib roughness height (e) to hydraulic diameter (D_h) ratio (e/D_h) and rise in temperature parameter on thermal efficiency.

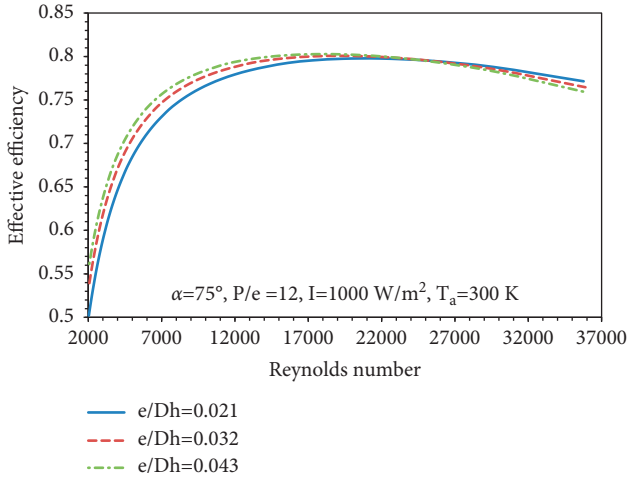

Figure 10: Impact of rib roughness height (e) to hydraulic diameter (D_h) ratio (e/D_h) on effective thermal efficiency of IRTDSAH.

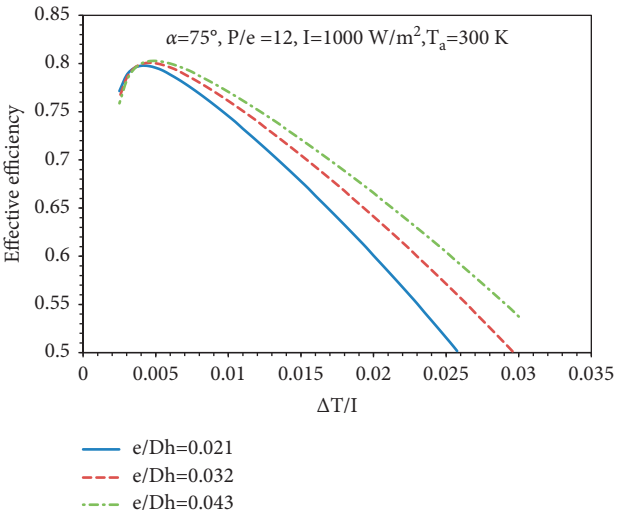

Figure 11: Impact of rib roughness height (e) to hydraulic diameter (D_h) ratio (e/D_h) and rise in temperature parameter on the effective thermal efficiency of IRTDSAH.

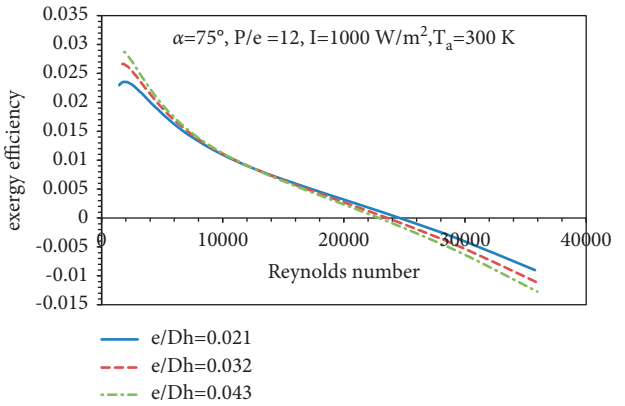

Figure 12: Impact of rib roughness height (e) to hydraulic diameter (D_h) ratio (e/D_h) on the effective thermal efficiency of IRTDSAH.

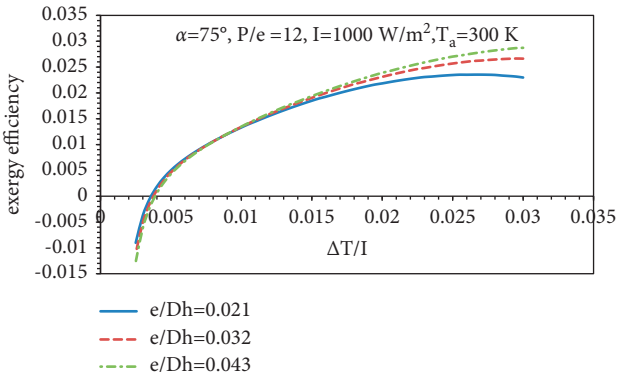

Figure 13: Impact of rib roughness height (e) to hydraulic diameter (D_h) ratio (e/D_h) on exergy thermal efficiency of IRTDSAH.

values were found to increase with the increase in e/D_h. The maximum thermal efficiency value found in the analysis is 83.61% at $e/D_h = 0.043$. Comparatively, at higher relative roughness height, the thermal efficiency is higher because of

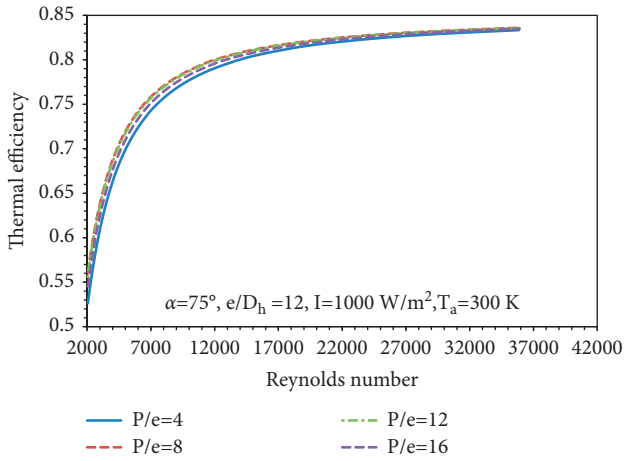

Figure 14: Impact of roughness pitch (p) to height (e) ratio (p/e) and Reynolds number on the thermal efficiency of IRTDSAH.

the effective breaking of thermal barrier formulated in fluid boundaries.

Figure 10 reveals the impact of rib roughness height (e) to hydraulic diameter (D_h) ratio (e/D_h) ranges from 0.021 to 0.043 on effective thermal efficiency of IRTDSAH, while flowing of air at the Reynolds number from 2000 to 35000, and maintaining other roughness parameters are constant, i.e., $\alpha = 75^{\circ}$ and $P/e = 12$. The effective efficiency values found increase up to the critical Reynolds Number, as shown in Table 6. The maximum effective efficiency value found in the analysis is 80.26% in $e/D_h = 0.043$ at 17534 Reynolds number. For the same Reynolds number with $e/D_h = 0.021$, the effective efficiency is 79.76%, while the trend gets reversed at higher Reynolds numbers (>25000) that $e/D_h = 0.021$ yield better performance due to offering lesser flow resistance and consumption lower pumping power. At a higher Reynolds number, the pressure drop increases due to the increment in roughness size increasing the pressure drop. Due to this reason, there is a dip in effective efficiency after the 17534 Reynolds Number. Comparatively, at higher relative roughness height, the effective efficiency is higher, which is evident.

Figure 11 reveals the impact of rib roughness height (e) to hydraulic diameter (Dh) ratio (e/D_h) ranging from 0.021 to 0.043 on the effective thermal efficiency of IRTDSAH while producing hot air with a rise in temperature parameter value ranging from 0.001 to 0.03 K·m^2/W, and maintaining other roughness parameters are constant, i.e., $\alpha = 75^{\circ}$ and $P/e = 12$. The effective efficiency values found increase up to the critical value of rising in temperature parameter as shown in Table 7. The maximum effective efficiency value found in the analysis is 80.26% at $e/D_h = 0.043$. Comparatively, at higher roughness height, the effective efficiency is higher.

Figure 12 reveals the impact of rib roughness height (e) to hydraulic diameter (D_h) ratio (e/D_h) on the exergy efficiency of IRTDSAH while flowing air at the Reynolds number from 2000 to 35000 and maintaining other roughness parameters that are constant, i.e., $\alpha = 75^{\circ}$ and $P/e = 12$. The exergy efficiency values found to increase up to the critical value of the Reynolds number, as shown in

Table 6: Critical Reynolds number based on different values of e/D_h.

S. n	e/D_h	Maximum effective efficiency (%)	Reynolds number
1	0.021	79.76	21937
2	0.032	80.07	19503
3	0.043	80.26	17534

Table 7: Influence of e/D_h on temperature parameter.

S. n	e/D_h	$\Delta T/I$ for maximum effective efficiency	Reynolds number
1	0.021	0.004	21937
2	0.032	0.0045	19503
3	0.043	0.005	17534

Table 8: Critical Reynolds number based on different values of e/D_h.

S. n	e/D_h	Maximum exergy efficiency (%)	Reynolds number
1	0.021	2.35	1850
2	0.032	2.66	1774
3	0.043	2.87	1864

Table 8. The maximum exergy efficiency value found in the analysis is 2.87% at $e/D_h = 0.043$ and at Re of 1864, and a further rise in Re > 1864 reduces the exergy efficiency. Comparatively, at operating the air heater lower rib roughness height (e) to hydraulic diameter (D_h) ratio declines the second law efficiency of the system due to higher exergy losses and destructions at a lower Reynolds number. At the system operated at a Reynolds number >20000, it produces a negative value of exergy efficiency for all the values of e/D_h due to the rise in internal exergy destruction parameters such as fluid friction occurs between absorber plate and working fluid.

Figure 13 reveals the impact of rib roughness height (e) to hydraulic diameter (D_h) ratio (e/D_h) ranging from 0.021 to 0.043 on exergy efficiency of IRTDSAH, while producing hot air with a rise in temperature parameter value ranges from 0.001 to 0.03 K·m^2/W, and maintaining other roughness parameters are constant, i.e., $\alpha = 75^{\circ}$ and $P/e = 12$. The exergy efficiency values were found to increase with the increase in $\Delta T/I$ and α till $\Delta T/I$ 0.03 K·m^2/W. The maximum exergy efficiency value found in the analysis is 2.87% at $e/D_h = 0.043$. Comparatively, at higher e/D_h the exergy efficiency is higher. It is observed that at higher $\Delta T/I$ the exergy efficiency value increases.

4.3. Effect of Roughness Pitch (P)-to-Height (e) Ratio (p/e) on Thermal Performance of IRTDSAH. The wire ribs are mounted on the IRTDSAH absorber plate with roughness pitch (p) to height (e) ratio (p/e) varies from 4 to 16, and its effects on the thermal effective thermal and exergy efficiency are shown in Figures 13–17.

Figure 14 reveals the impact of rib roughness pitch (p) to height (e) ratio (p/e) ranging from 4 to 16 on the thermal

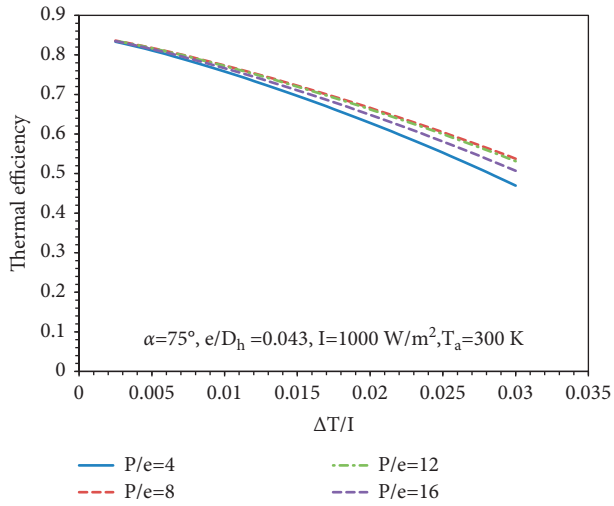

Figure 15: Impact of roughness pitch (p) to height (e) ratio (p/e) and rise in temperature parameter on the thermal efficiency of IRTDSAH.

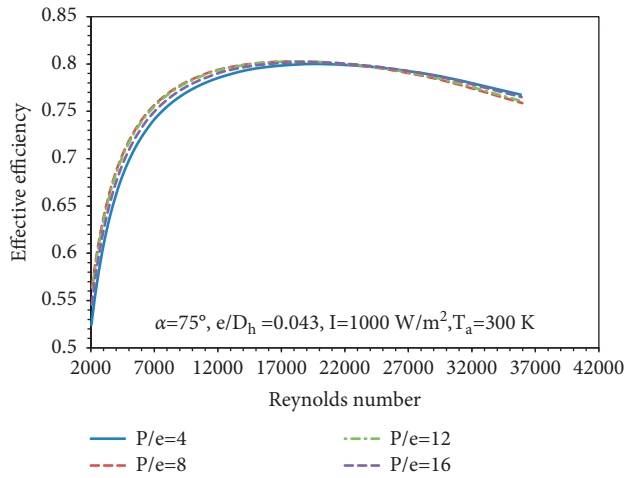

Figure 16: Impact of rib roughness pitch (p) to height (e) ratio (p/e) and Reynolds number on the effective thermal efficiency of IRTDSAH.

efficiency of IRTDSAH while flowing of air at the Reynolds number from 2000 to 35000 and maintaining other roughness parameters are constant, i.e., $e/D_h = 0.043$ and $\alpha = 75^\circ$. While increasing the Reynolds number from 2000 to 35000, the thermal efficiency of IRTDSAH improved by a maximum of 53.1% to 83.8% for the rib roughness pitch (p) to height (e) ratio (p/e) value of 12. While increasing or decreasing the value of P/e value of 12 decreases the thermal performance of IRTDSAH due to the formulation of sluggish boundary layers.

Figure 15 exemplifies the impact of roughness pitch (p) to height (e) ratio (p/e) on the thermal efficiency of IRTDSAH while producing hot air with a rise in temperature parameter value ranging from 0.001 to 0.03 K·m^2/W and maintaining other roughness parameters are constant, i.e., $e/D_h = 0.043$ and $\alpha = 75^\circ$. The thermal efficiency values were found to increase with the increase in p/e value up to 12 and

Table 9: Critical Reynolds number based on different values of P/e.

S. n	P/e	Maximum effective efficiency (%)	Reynolds number
1	4	80	19469
2	8	80.1	17522
3	12	80.22	17534
4	16	80.17	19527

achieving the maximum thermal efficiency value of 83.61%. Comparatively providing the p/e of 12 improves the thermal efficiency because of the increase in reattachment points in the boundary layer and enriching the local heat transfer coefficients.

Figure 16 rib roughness pitch (p) to height (e) ratio (p/e) ranges from 4 to 16 on the effective thermal efficiency of IRTDSAH, while flowing of air at the Reynolds number from 2000 to 35000, and maintaining other roughness parameters are constant, i.e., $\alpha = 75^\circ$ and $e/D_h = 0.043$. The effective efficiency values found increase up to the critical Reynolds Number, as shown in Table 9. The maximum effective efficiency value found in the analysis is 80.26% in $P/e = 12$ at the Reynolds number of 17534.

For the same Reynolds number with $P/e = 4$, the effective efficiency is 80%, while the trend gets reversed at higher Reynolds numbers (>25000) that $P/e = 4$ yield better performance due to offering of lesser flow resistance and consumption of lower pumping power. At a higher Reynolds number, the frictional resistance increases due to the increment in the number of elements, increasing the pressure drop. Due to this reason, there is a dip in effective efficiency after the 17534 Reynolds Number.

Figure 17 reveals the impact rib roughness pitch (p) to height (e) ratio (p/e) ranges from 4 to 16 on the effective thermal efficiency of IRTDSAH, while producing hot air with a rise in temperature parameter value ranges from 0.001 to 0.03 K·m^2/W, and maintaining other roughness parameters are constant, i.e., $\alpha = 75^\circ$ and $e/D = 0.043$. The effective efficiency values found increase up to the critical value of rise in temperature parameter as shown in Table 10. The maximum effective efficiency value found in the analysis is 80.26% at $P/e = 12$.

Figure 18 reveals the impact of rib roughness pitch (p) to height (e) ratio (p/e) on the exergy efficiency of IRTDSAH while flowing of air at the Reynolds number from 2000 to 35000, and maintaining other roughness parameters are constant, i.e., $\alpha = 75^\circ$ and $e/D_h = 0.042$. The exergy efficiency values were found to increase up to the critical value of the Reynolds number, as shown in Table 11. The maximum exergy efficiency value found in the analysis is 2.87% at $P/e = 12$ at the Re of 1864 and a further rise in Re > 1864 reduces the exergy efficiency.

Figure 19 reveals the impact rib roughness pitch (p) to height (e) ratio (p/e) ranging from 4 to 16 on exergy efficiency of IRTDSAH while producing hot air with a rise in temperature parameter value ranging from 0.001 to 0.03 K·m^2/W and maintaining other roughness parameters are constant, i.e., $\alpha = 75^\circ$ and $e/D = 0.043$. The exergy efficiency values were found to increase with the increase in $\Delta T/$

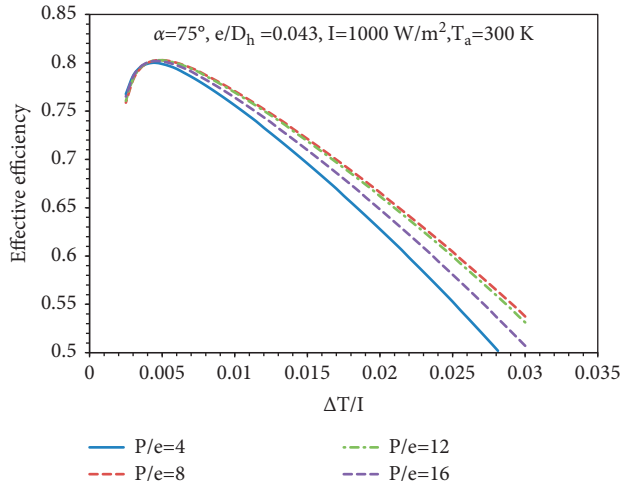

Figure 17: Impact of rib roughness pitch (p) to height (e) ratio (p/e) and rise in temperature parameter on the effective thermal efficiency of IRTDSAH.

Table 10: Influence of P/e on temperature parameter.

S. n	P/e	$\Delta T/I$ for maximum effective efficiency	Reynolds number
1	4	0.0045	19469
2	8	0.005	17522
3	12	0.005	17534
4	16	0.0045	19527

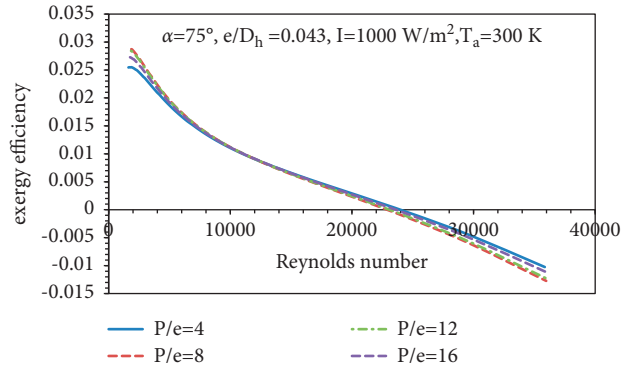

Figure 18: Impact of rib roughness pitch (p) to height (e) ratio (p/e) and Reynolds number on the effective thermal efficiency of IRTDSAH.

Table 11: Critical Reynolds number based on different values of P/e.

S. n	P/e	Maximum exergy efficiency (%)	Reynolds number
1	4	2.54	1878
2	8	2.63	1864
3	12	2.87	1843
4	16	2.72	1759

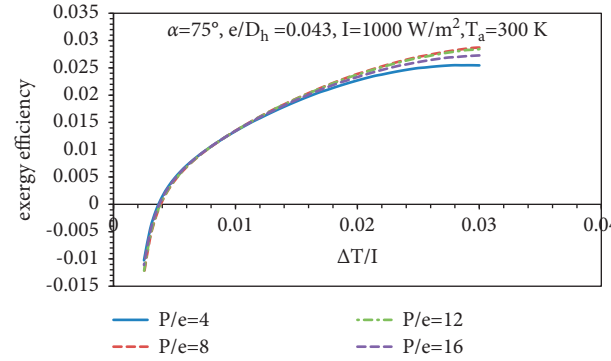

Figure 19: Influence of rib roughness pitch (p) to height (e) ratio (p/e) on the rise in temperature parameter on exergy thermal efficiency of IRTDSAH.

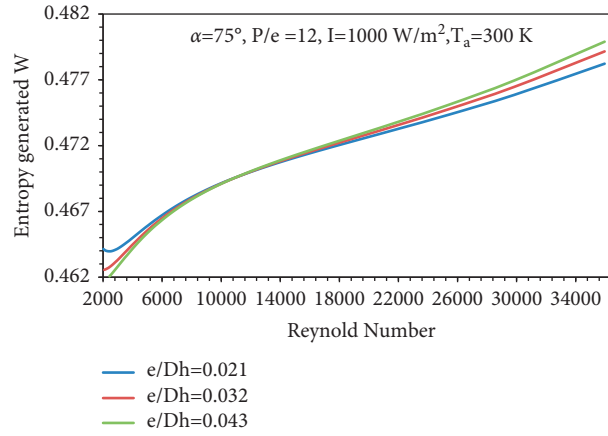

Figure 20: Influence of rib roughness height (e) ratio to hydraulic diameter (e/D_h) and Reynolds number on entropy generation of IRTDSAH.

I and α till ΔT/I 0.03 K·m^2/W. The maximum exergy efficiency value found in the analysis is 2.87% at $e/D_h = 0.043$. Comparatively, at higher p/e up to 12, the exergy efficiency is higher.

4.4. Entropy Generation. The influence of e/D_h value on entropy generation is described in Figure 20. From the figure, it is observed that the e/D_h value of 0.043 produces a lower value of entropy for the Re ranging from 2000 to 6000. Then increase in flow rate rise value of entropy generation and the maximum value destruction occurs during the operating condition that consists of the e/D_h value of 0.021.

5. Conclusion

In the present work, circular wire ribs attached over an absorber plate in an inclined manner act as an artificial roughness for a triangular duct solar air heater. The analytical model is used to evaluate the optimum dimensions of the roughness dimensions relative roughness height of 0.021–0.043, relative roughness pitch of 4–16 and inclination angle of the arc of 30 to 75°. From the analytical results, it is concluded that

(i) While increasing the roughness pitch (P) to height (e) ratio (P/e), roughness height (e) to hydraulic diameter (D_h) ratio (e/D_h), rib inclination angle (α), and mass flow rate improve the thermal performance of the system. It is also noticed that the exergy performance of IRTDSAH decreases with the increase in Reynolds number > 1864

(ii) The maximum thermal efficiency of 83.61% is obtained at P/e of 12, e/D of 0.042, and α of 75°. It is founded that the thermal efficiency is increased with the rise in all these parameters and obtains its maximum value at Re of 35000

(iii) The effective thermal efficiency attains its maximum value of 80.26% at the Re of 17543 with the roughness parameters ranges of P/e of 12, e/D of 0.042, and α of 75°

(iv) The maximum exergy efficiency of 2.62% is attained at the Re of 1864 at the optimized operating conditions. The air heater can produce a rise in temperature value 0.005 to 0.03 K·m^2/W as compared with other systems. The exergy based parameter optimization yields more accurate results to fix the roughness parameters

Nomenclature

Ac: Area of the collector
C_{pf}: Specific heat of air (J/kg K)
D_h: Triangular tube hydraulic diameter (m)
F_R: Triangular heater heat removal factor
Fr: Friction at triangular channel
h: Convective heat transfer coefficient (W/m^{2}K)
I: Solar radiation (W/m^2)
k: Thermal conductivity (W/m K)
L: Length of the triangular duct (m)
m: Mass flow rate (kg/s)
Nu: Nusselt number
P_m: Pumping power (W)
Q_u: Useful heat gain (W)
Re: Reynolds number
T: Temperature (K)
tg: Thickness of glass (m)
UL: Overall loss coefficient (W/mK)
W: Width of the duct (9 m)

Greek symbols
μ: Viscosity (Ns m^{-2})
ρ: Density (kg/m^3)
ε: Emissivity
α_τ: Product of transmittance and absorptance
β: Tilt angle (°)
η: Efficiency (%)
δ: Thickness of insulation (m)

Subscripts
a: Ambient air
c: Convection
g: Glass
p: Plate
i: Inlet
o: Outlet

Abbreviations
SAH: Solar air heater
IRTDSAH: Inclined rib roughened triangular duct solar air heater.

Data Availability

The data used to support the findings of this study are included within the article.

Conflicts of Interest

The authors declare that there are no conflicts of interest regarding the publication of this article.

References

[1] S. H. Farjana, N. Huda, M. A. P. Mahmud, and R. Saidur, "Solar process heat in industrial systems - a global review," *Renewable and Sustainable Energy Reviews*, vol. 82, pp. 2270–2286, 2018.

[2] V. Manoj Praveen, R. Vigneshkumar, N. Karthikeyan, A. Gurumoorthi, R. Vijayakumar, and P. Madhu, "Heat transfer enhancement of air-concrete thermal energy storage system - CFD simulation and experimental validation under transient condition," *Proceedings of the Institution of Mechanical Engineers - Part E: Journal of Process Mechanical Engineering*, vol. 235, no. 5, pp. 1304–1314, 2021.

[3] N. S. Suresh and B. S. Rao, "Solar energy for process heating: a case study of select Indian industries," *Journal of Cleaner Production*, vol. 151, pp. 439–451, 2017.

[4] V. Singh Bisht, A. Kumar Patil, and A. Gupta, "Review and performance evaluation of roughened solar air heaters," *Renewable and Sustainable Energy Reviews*, vol. 81, pp. 954–977, 2018.

[5] C.-S. Wang, C.-C. Chen, W.-C. Chang, and T.-M. Liou, "Experimental studies of turbulent pulsating flow and heat transfer in a serpentine channel with winglike turbulators," *International Communications in Heat and Mass Transfer*, vol. 131, Article ID 105837, 2022.

[6] P. Promvonge, P. Promthaisong, and S. Skullong, "Experimental and numerical thermal performance in solar receiver heat exchanger with trapezoidal louvered winglet and wavy groove," *Solar Energy*, vol. 236, pp. 153–174, 2022.

[7] G. Verma, S. Singh, S. Chander, and P. Dhiman, "Numerical investigation on transient thermal performance predictions of phase change material embedded solar air heater," *Journal of Energy Storage*, vol. 47, Article ID 103619, 2022.

[8] R. Kumar, A. Varun, and A. Kumar, "Thermal and fluid dynamic characteristics of flow through triangular cross-sectional duct: a review," *Renewable and Sustainable Energy Reviews*, vol. 61, pp. 123–140, 2016.

[9] V. Goel, P. Guleria, and R. Kumar, "Effect of apex angle variation on thermal and hydraulic performance of roughened triangular duct," *International Communications in Heat and Mass Transfer*, vol. 86, pp. 239–244, 2017.

[10] R. Kumar, A. Kumar, and V. Varun, "Computational fluid dynamics based study for analyzing heat transfer and friction factor in semicircular rib-roughened equilateral triangular duct," *International Journal of Numerical Methods for Heat and Fluid Flow*, vol. 27, no. 4, pp. 941–957, 2017.

[11] R. Kumar, A. Varun, and A. Kumar, "Experimental and computational fluid dynamics study on fluid flow and heat transfer in triangular passage solar air heater of different configurations," *Journal of Solar Energy Engineering*, vol. 139, no. 4, Article ID 041013, 2017.

[12] R. Kumar, A. Kumar, and V. Goel, "A parametric analysis of rectangular rib roughened triangular duct solar air heater using computational fluid dynamics," *Solar Energy*, vol. 157, pp. 1095–1107, 2017.

[13] G. Bharadwaj, R. Varun Kumar, R. Kumar, and A. Sharma, "Heat transfer augmentation and flow characteristics in ribbed triangular duct solar air heater: an experimental analysis," *International Journal of Green Energy*, vol. 14, no. 7, pp. 587–598, 2017.

[14] S. Singh, "Thermal performance analysis of semicircular and triangular cross-sectioned duct solar air heaters under external recycle," *Journal of Energy Storage*, vol. 20, pp. 316–336, 2018.

[15] R. Kumar, V. Goel, A. Kumar, S. Khurana, P. Singh, and S. B. Bopche, "Numerical investigation of heat transfer and friction factor in ribbed triangular duct solar air heater using Computational fluid dynamics (CFD)," *Journal of Mechanical Science and Technology*, vol. 32, no. 1, pp. 399–404, 2018.

[16] R. Kumar, S. Khurana, A. Kumar, and V. Goel, "Effect of dimple intrusions and curvature radius of rounded corner triangular duct on fluid flow and heat transfer," *Journal of Thermal Science and Engineering Applications*, vol. 11, no. 3, Article ID 031001, 2019.

[17] R. Kumar, A. Kumar, and V. Goel, "Effect of rounded corners on heat transfer and fluid flow through triangular duct," *Journal of Heat Transfer*, vol. 140, no. 12, Article ID 121709, 2018.

[18] S. K. Jain, G. D. Agrawal, R. Misra, P. Verma, S. Rathore, and D. K. Jamuwa, "Performance investigation of a triangular solar air heater duct having broken inclined roughness using computational fluid dynamics," *Journal of Solar Energy Engineering*, vol. 141, no. 6, Article ID 061008, 2019.

[19] K. Nidhul, S. Kumar, A. K. Yadav, and S. Anish, "Enhanced thermo-hydraulic performance in a V-ribbed triangular duct solar air heater: CFD and exergy analysis," *Energy*, vol. 200, Article ID 117448, 2020.

[20] R. Misra, J. Singh, S. K. Jain et al., "Prediction of behavior of triangular solar air heater duct using V-down rib with multiple gaps and turbulence promoters as artificial roughness: a CFD analysis," *International Journal of Heat and Mass Transfer*, vol. 162, Article ID 120376, 2020.

[21] K. Nidhul, S. Kumar, A. K. Yadav, and S. Anish, "Influence of rectangular ribs on exergetic performance in a triangular duct solar air heater," *Journal of Thermal Science and Engineering Applications*, vol. 12, no. 5, Article ID 051010, 2020.

[22] S. Kumar, R. Kumar, V. Goel, S. Bhattacharyya, and A. Issakhov, "Exergetic performance estimation for roughened triangular duct used in solar air heaters," *Journal of Thermal Analysis and Calorimetry*, vol. 145, no. 3, pp. 1661–1672, 2021.

[23] M. K. Sahu and R. K. Prasad, "Exergy based performance evaluation of solar air heater with arc-shaped wire roughened absorber plate," *Renewable Energy*, vol. 96, pp. 233–243, 2016.

[24] R. Chauhan and N. S. Thakur, "Investigation of the thermohydraulic performance of impinging jet solar air heater," *Energy*, vol. 68, pp. 255–261, 2014.

[25] M. M. Matheswaran, T. V. Arjunan, and D. Somasundaram, "Analytical investigation of solar air heater with jet impingement using energy and exergy analysis," *Solar Energy*, vol. 161, pp. 25–37, 2018.

[26] M. M. Matheswaran, T. V. Arjunan, and D. Somasundaram, "Energetic, exergetic and enviro-economic analysis of parallel pass jet plate solar air heater with artificial roughness," *Journal of Thermal Analysis and Calorimetry*, vol. 136, no. 1, pp. 5–19, 2019.

[27] M. K. Sahu, M. M. Matheswaran, and P. Bishnoi, "Experimental Investigation of Augmented thermal and performance Characteristics of Solar Air Heater Ducts Due to Varied Orientations of Roughness Geometry on the Absorber Plate," *Archives of Thermodynamics*, vol. 41, pp. 147–182, 2020.

[28] M. Matheswaran, T. Arjunan, and M. K. Sahu, "Influence of twisted tape fins on heat transfer and friction factor characteristics for impinging jet solar air heater," *Proceedings of the Institution of Mechanical Engineers - Part E: Journal of Process Mechanical Engineering*, vol. 235, no. 4, pp. 824–831, 2021.